Analytical and Bioanalytical Chemistry (2022) 414:2355–2362
https://doi.org/10.1007/s00216-021-03858-8

RESEARCH PAPER

A Ti_3C_2-MXene-functionalized LRSPR biosensor based on sandwich amplification for human IgG detection

Xueqi Zhao[1] · Yue Zhang[1] · Xinghua Wang[1] · Pinyi Ma[1] · Daqian Song[1] · Ying Sun[1]

Received: 1 November 2021 / Revised: 1 December 2021 / Accepted: 20 December 2021 / Published online: 16 February 2022

Abstract

Long-range surface plasmon resonance (LRSPR) has demonstrated excellent performance in sensing and detection, due to its higher accuracy and sensitivity compared with conventional surface plasmon resonance (cSPR). In this work, we establish an LRSPR biosensor which employs PDA/Ti_3C_2-MXene/PDA-gold film as a sensing substrate and gold nanoparticles (AuNPs) as enhancers. Ti_3C_2-MXene is an emerging two-dimensional (2D) layered material which is used extensively in immunoassay and biosensing. The sensing substrate comprises two polydopamine (PDA) films between which is sandwiched a Ti_3C_2-MXene film based on a gold film, which provides a large surface area and abundant binding sites to rabbit anti-human IgG (Ab_1). Sandwich amplification is adopted to enhance the sensitivity of the LRSPR biosensor, and AuNPs/staphylococcal protein A (SPA)/mouse anti-human IgG (Ab_2) composites are introduced into the flow cell as enhancers after the immune binding of human IgG to Ab_1. The antigen (human IgG) detection range is 0.075 μg mL^{-1} to 40 μg mL^{-1}, and the limit of detection is almost 20 times lower than that for cSPR biosensors. This novel LRSPR biosensor demonstrates excellent performance in immune sensing over a broad detection range and a low limit of detection. Subsequent modification of the LRSPR sensing platform could be made for extensive application in various biological detection fields.

Keywords LRSPR · Ti_3C_2-MXene · Sandwich amplification · Gold nanoparticles (AuNPs)

Introduction

Long-range surface plasmon resonance (LRSPR) is a type of surface plasmon resonance (SPR) which can be produced on a thin metal film inserted between an analyte medium and a buffer medium with a similar refractive index (RI) [1]. Sarid [2] proposed the concept in 1981, and since then a number of theoretical and practical studies have led to continuous improvement in the performance of LRSPR. The unique feature of LRSPR is the dielectric buffer layer (DBL) between the metal film and substrate, which contributes to longer penetration depth of plasmonic waves compared with conventional SPR (cSPR). To date, various DBL materials have been developed with low RI, such as Teflon [3], Cytop [4], plasma-polymerized (perfluorooctyl)ethylene (pp-PFOE) [5], AlF_3 [6], LiF [7], MgF_2 [1], and SiO_2 [8]. LRSPR exhibits longer surface-wave propagation distance and higher sensitivity and accuracy than cSPR. In this respect, LRSPR has demonstrated excellent biosensing performance, including ABO blood typing [9], toxicity tests based on living cells [10], imaging for bioaffinity sensors [11], and detection of carcinoembryonic antigen (CEA) [12], mycotoxin [13], dengue NS1 antigen [14, 15], HER2 breast cancer biomarker [16], and other small molecules [17].

Based on the excellent characteristics of LRSPR technology, two-dimensional (2D) laminated nanomaterials such as graphene, MXenes [18], and transition metal dichalcogenides (TMDCs) [19] have been used to modify the LRSPR sensing platform. MXenes are a group of compounds comprising transition metal nitrides, carbonitrides, and carbides, which are generally prepared by etching from corresponding MAX phases [20]. MAX phases have a composition that follows the general formula $M_{n+1}AX_n$ (n = 1, 2, 3), where M represents early transition metals such as Ti, V, Cr, Sr, Nb, or Ta; A corresponds to a group A element, most likely groups 13 and 14 in the periodic table; and X corresponds to carbon or nitrogen [21, 22]. Ti_3C_2-MXene represents an emerging

✉ Ying Sun
yingsun@jlu.edu.cn

[1] College of Chemistry, Jilin Province Research Center for Engineering and Technology of Spectral Analytical Instruments, Jilin University, Qianjin Street 2699, Changchun 130012, China

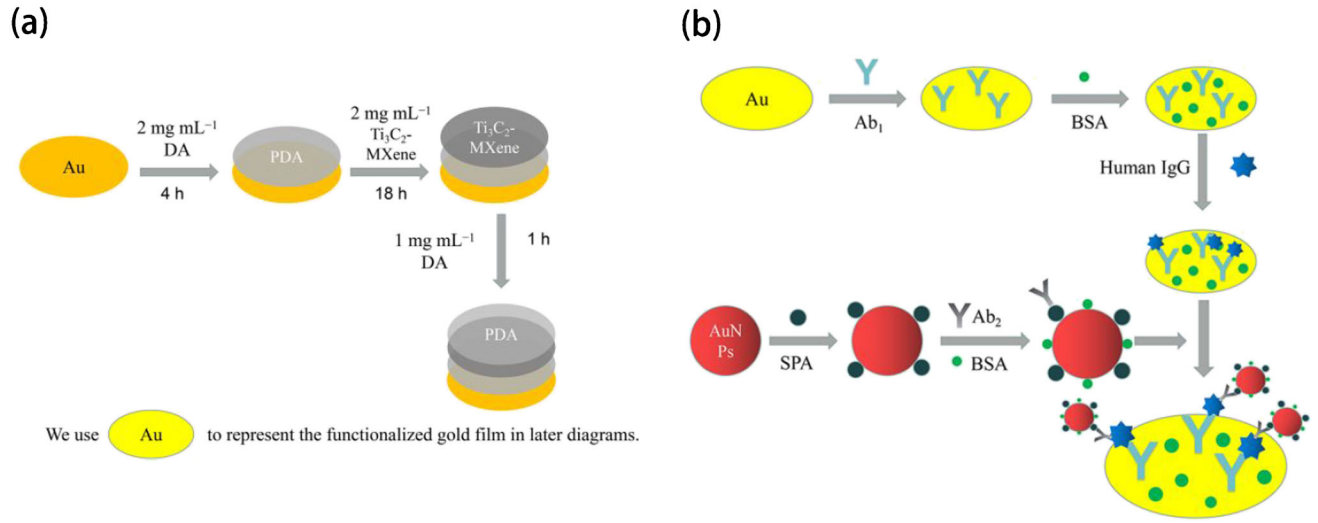

Fig. 1 Schematic of detection procedure of the prepared LRSPR biosensor. **a** The preparation of PDA/Ti_3C_2-MXene/PDA gold films. **b** Ab_1 was immobilized on the modified gold film, and AuNPs/SPA/Ab_2 composites were introduced as signal enhancers

nanomaterial with abundant hydroxyl, oxygen, and metal atomic functional groups on the surface, leading to plentiful binding sites, high capacity, strong stability, ease of modification, and excellent biocompatibility [18]. Therefore, Ti_3C_2-MXene has been employed extensively in SPR biosensors [21], electrochemical biosensors [22], capacitance immunoassay [23], self-assembled layers for batteries [24], and dielectric materials, with excellent properties [25].

However, due to the constriction of sensitivity and detection limit, modification of the sensing substrate and application of nanoparticles for secondary amplification are commonly used to enhance the response signal of LRSPR biosensors. The unique coating properties and rich functional groups on the surface of polydopamine (PDA) make it a promising biosensing material due to its large specific surface area, excellent biocompatibility, and stable structure [26]. Meanwhile, as commonly used nanoparticles, gold nanoparticles (AuNPs) exhibit unique photoelectric and chemical properties coupled with localized surface plasmon resonance (LSPR), and are widely employed in the detection of biological and drug molecules [27, 28].

In this paper, we propose a novel LRSPR biosensor based on a 350 nm MgF_2 layer embedded between a 50 nm gold layer and K9 glass to detect human IgG. The Ti_3C_2-MXene nanolayer sandwiched between PDA layers with different thickness was assembled on the surface of gold film serving as a biosensing substrate to enhance sensitivity and bind rabbit anti-human IgG (Ab_1). The AuNPs were decorated with staphylococcal protein A (SPA) for oriented immobilization of mouse-anti-human IgG (Ab_2). AuNPs/SPA/Ab_2 nanocomposites were introduced into the LRSPR biosensor for signal amplification. The results revealed higher sensitivity and a lower detection limit in the detection of human IgG compared to ordinary LRSPR biosensors and cSPR biosensors. The LRSPR biosensor based on Ti_3C_2-MXene therefore represents a promising tool for clinical immunoassay in the future.

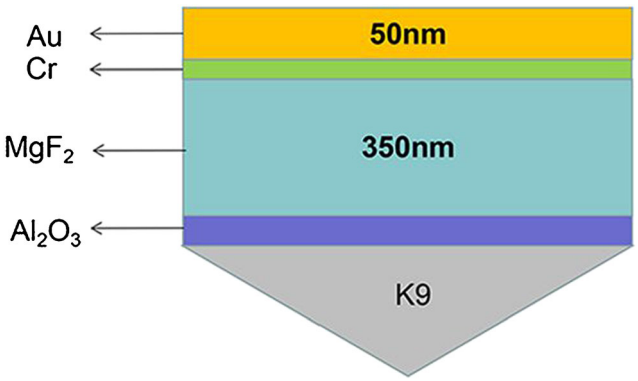

Fig. 2 Structure of LRSPR sensing substrate. The original gold film mainly consisted of a 50 nm gold layer and 350 nm MgF_2 layer

Material and methods

Materials and instruments

Dopamine hydrochloride (DA), titanium carbide MXene thin-layer dispersion (Ti_3C_2-MXene), gold(III) chloride trihydrate ($HAuCl_4 \cdot 3H_2O$), and 1-(3-dimethylaminopropyl)-3-ethylcarbodiimide hydrochloride (EDC) were purchased from Energy Chemical (https://www.energy-chemical.com). Trisodium citrate dihydrate ($C_6H_5Na_3O_7 \cdot 2H_2O$) was purchased from Sinopharm Chemical Reagent Co., Ltd. (https://shreagent.lookchem.com). Staphylococcal protein A (SPA) was purchased from Sigma-Aldrich (https://www.sigmaaldrich.cn). *N*-hydroxysuccinimide (NHS) and 3-mercaptopropionic acid

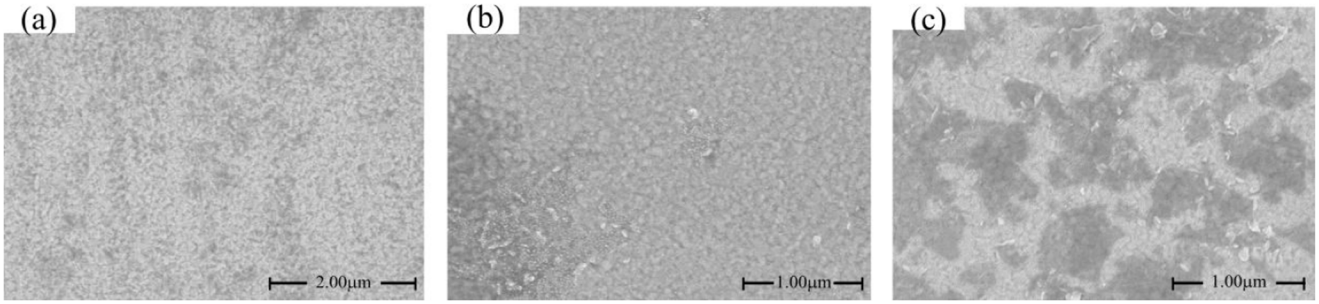

Fig. 3 SEM images of **a** PDA-gold film, **b** Ti_3C_2-MXene/PDA-gold film, and **c** PDA/Ti_3C_2-MXene/PDA gold film

(MPA) were purchased from Aladdin (https://www.aladdin-e.com). Bovine serum albumin (BSA) was purchased from Beijing Aobox Biotechnology Co., Ltd. (https://bjabx.company.lookchem.cn). Rabbit anti-human IgG, mouse anti-human IgG, human IgG, mouse IgG, and bovine IgG were purchased from Beijing Biosynthesis Biotechnology Co., Ltd. (http://www.bioss.com.cn). Human serum was purchased from Beijing Solarbio Science & Technology Co., Ltd. (https://solarbio.en.alibaba.com). Sodium phosphate-buffered saline (PBS, 0.01 mol L^{-1}, pH = 7.4) and Tris buffer (0.01 mol L^{-1}, pH = 8.5) were prepared before the experiments. Rabbit anti-human IgG, mouse anti-human IgG, human IgG, mouse IgG, bovine IgG, and bovine serum were stored at −20 °C. MPA and $C_6H_5Na_3O_7{\cdot}2H_2O$ were stored at room temperature. The other materials were stored at 4 °C.

LRSPR experiments were carried out via a wavelength modulation SPR instrument based on the Kretschmann configuration assembled by our research group.

Pretreatment of biosensing platform

The LRSPR structure consisted of a 350 nm MgF_2 layer and a 50 nm gold layer. Cr and Al_2O_3 served as connectors.

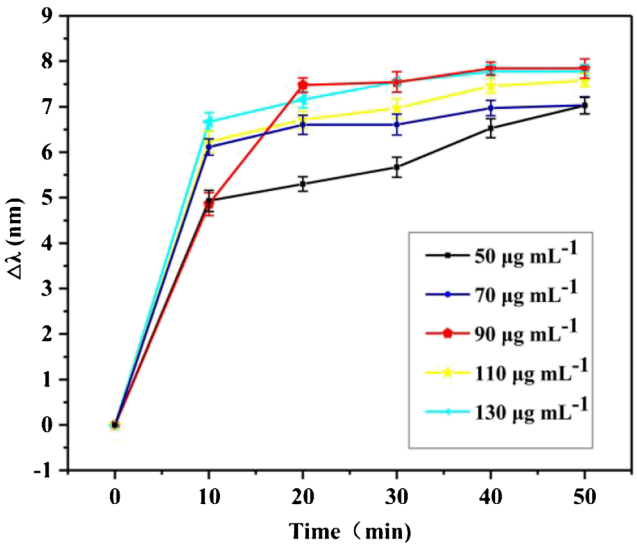

Fig. 4 Kinetic adsorption curves of Ab_1 at different concentrations. The optimal concentration of Ab_1 was 90 μg mL^{-1}. Error bar = ±SD and n = 3

The bare gold film was successively rinsed in ethanol and deionized (DI) water, and then dried under nitrogen (N_2). The cleaned gold film was immersed in 2 mg mL^{-1} DA solution (dissolved in Tris buffer) for 4 h to self-assemble a PDA layer on its surface. The PDA-gold film was then rinsed with DI water and dried with N_2. The film was immersed in 2 mg mL^{-1} Ti_3C_2-MXene solution (dissolved in DI water) for 18 h to obtain the second self-assembled layer, followed by the same cleaning method as for the first layer. Finally, the Ti_3C_2-MXene/PDA-gold film was immersed in 1 mg mL^{-1} DA solution (dissolved in Tris buffer) for 1 h to self-assemble the last layer, followed by cleaning as above. The PDA/Ti_3C_2-MXene/PDA-gold films were prepared in advance.

Immobilization of rabbit anti-human IgG

The prepared modified gold film was fixed on a prism to form a flow cell with the reactor of the SPR instrument. PBS was injected into the flow cell to adjust the baseline, and 90 μg mL^{-1} (0.5 mL, PBS) Ab_1 was injected and incubated for 40 min. The amine groups on Ab_1 reacted with the quinone groups on PDA for Schiff–base reaction [29]. After that, unbound Ab_1 was washed away with PBS, and 10 mg mL^{-1} BSA was injected to block nonspecific binding sites on the surface of the platform for 20 min. Finally, residual BSA was washed away with PBS.

Synthesis of AuNPs/SPA/Ab_2 nanocomposites

We used a chemical reduction based on citrate for $HAuCl_4$ to prepare the AuNPs. A total of 48.5 μL of $HAuCl_4{\cdot}3H_2O$ solution (0.1 g mL^{-1}) was added to 50 mL of ultra-pure water in a round flask and heated to micro-boiling. Then 0.5 mL $C_6H_5Na_3O_7{\cdot}2H_2O$ solution (1 wt%) was added to the above solution. The color of the solution turned blue after 25 s and suddenly turned bright red after 70 s. $HAuCl_4{\cdot}3H_2O$ reacted completely after micro-boiling for 5 min. The obtained AuNPs were centrifuged at 10,000 rpm for 20 min and redispersed in 10 mL DI water.

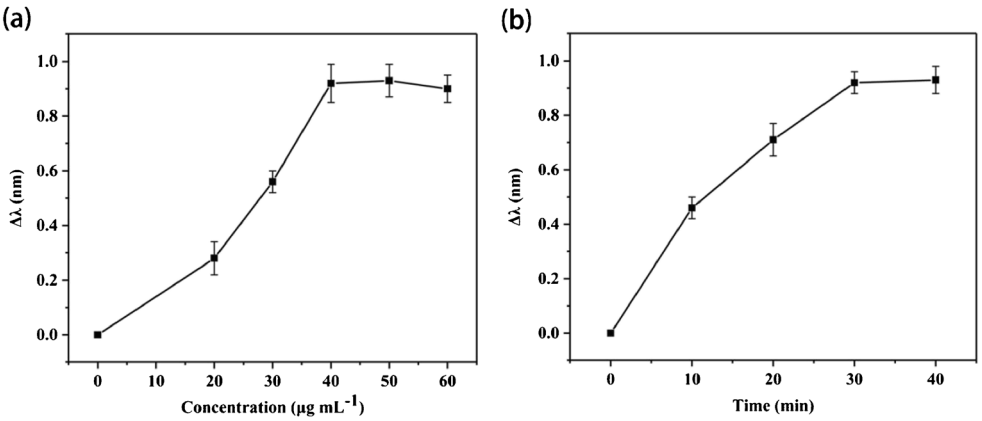

Fig. 5 Optimization of reaction conditions for **a** maximum concentration of human IgG and **b** fixed time of human IgG. The optimal concentration of human IgG was 40 μg mL^{-1} and the immobilization time was 30 min. Error bar = ±SD and n = 3

Nine hundred microliters of AuNPs and 100 μL SPA (1 mg mL^{-1}) were mixed and kept at 4 °C for 3 h, after which the solution was centrifuged to remove the residual SPA and redispersed in 1 mL PBS. Then 250 μL AuNPs/SPA and 50 μL Ab_2 (1 mg mL^{-1}) were mixed and kept at 4 °C overnight. The dose of AuNPs/SPA/Ab_2 was adjusted while keeping the concentration of human IgG and the volume ratio constant. SPA effectively combined Ab_2 and AuNPs through covalent bonding to yield AuNPs/SPA/Ab_2 stable composites. Ten microliters of BSA (10 mg mL^{-1}) was added to the mixed solution for blocking the nonspecific binding sites on the surface of the AuNPs.

Detection of human IgG

Five hundred microliters of human IgG (dissolved in PBS) with different concentrations was injected into the flow cell and incubated for 30 min on the sensing platform. Unbound human IgG was gently removed by washing with PBS. Then 500 μL AuNPs/SPA/Ab_2 solution was introduced into the flow cell to enhance the response signal. Unreacted AuNPs/SPA/Ab_2 was gently washed off with PBS. The resonant wavelength shifts were calculated from the injection of human IgG to the removal of unbound AuNPs/SPA/Ab_2. The experimental flow chart is illustrated in Fig. 1. All experiments were carried out three times to ensure accuracy.

LRSPR biosensors based on PDA-gold film and bare gold film were also used to detect human IgG for comparison experiments. The detection procedure for the PDA-gold film biosensor was the same as for the modified gold film biosensor. The immobilization of Ab_1 on the bare gold film biosensor was adjusted. Firstly, 10 mmol L^{-1} MPA was injected for 1 h after the baseline was stabilized by PBS. Then a mixture of 1.5 mmol L^{-1} NHS and 7.5 mmol L^{-1} EDC was injected to activate the carboxyl groups of MPA. The immobilization of Ab_1 and subsequent procedures were the same as above.

Results and discussion

PDA/Ti_3C_2-MXene/PDA-functionalized sensing substrate

As the first proposed wavelength modulation LRSPR biosensor, the structure is shown in Fig. 2, with a 350 nm MgF_2 layer and a 50 nm gold layer. Al_2O_3 and Cr were employed as connecting materials between the two adjacent layers. We chose MgF_2 as the material for the DBL because of its high

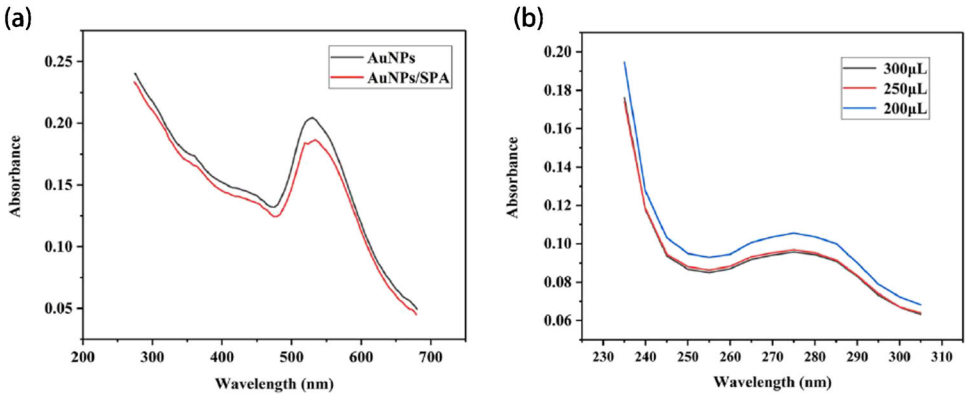

Fig. 6 UV-Vis absorption spectra of **a** AuNPs and AuNPs/SPA and **b** residual supernatant Ab_2 when the volume of AuNPs/SPA was 200 μL, 250 μL, and 300 μL, respectively. **a** The absorption peak of the AuNPs appeared at 530 nm and that of AuNPs/SPA at 534 nm. **b** The optimal volume ratio was 250 μL AuNPs/SPA to 50 μL Ab_2

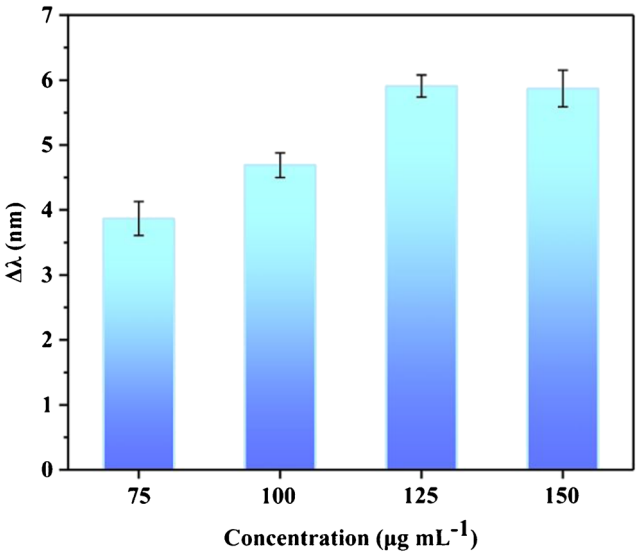

Fig. 7 Shifts of resonant wavelengths (Δλ) of AuNPs/SPA/Ab_2 containing different concentrations of Ab_2. The optimal concentration of Ab_2 in the AuNPs/SPA/Ab_2 composites was 125 μg mL^{-1}. Error bar = ±SD and n = 3

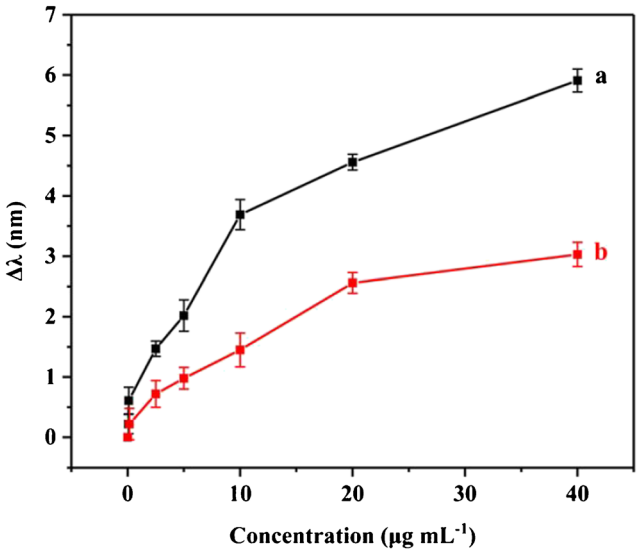

Fig. 9 Relationship between the shift of resonant wavelength (Δλ) and concentration of human IgG **a** with AuNPs/SPA/Ab_2 and **b** without AuNPs/SPA/Ab_2. Error bar = ±SD and n = 3

stability and ease of deposition, which makes it highly suitable for optical coating applications [30].

In general, increasing the surface area and increasing the number of binding sites are the most common methods used to enhance the sensitivity of LRSPR detection. Here, we adopted PDA and Ti_3C_2-MXene as a dual amplification strategy to increase the surface area and number of binding sites. The sensing substrate was preprocessed in advance to shorten the detection time. The gold film was successively immersed in DA, Ti_3C_2-MXene, and DA to self-assemble a thin film on top of the upper layer. DA can self-polymerize into PDA on top of most substances under alkaline conditions, due to the strong affinity of the catechol functional groups on it. The Schiff–base reaction between PDA and antibodies can effectively immobilize Ab_1. Scanning electron microscopy (SEM) images (Fig. 3) showed a uniform distribution, indicating that the three self-assembled layers were successfully formed. The energy-dispersive X-ray spectroscopy (EDS) image shown in Fig. S1 indicates that Ti_3C_2-MXene was modified on the gold film. The first PDA layer served as a linking layer between the gold film and the Ti_3C_2-MXene layer. The Ti_3C_2-MXene layer afforded a large surface area and high loading capacity for more binding sites. The last PDA layer was thinner than the first PDA layer and was mainly employed to provide binding sites for antibodies. These three layers were used to construct the sensing substrate in the sandwich layer model, to improve the performance and enhance the sensitivity of the LRSPR biosensor.

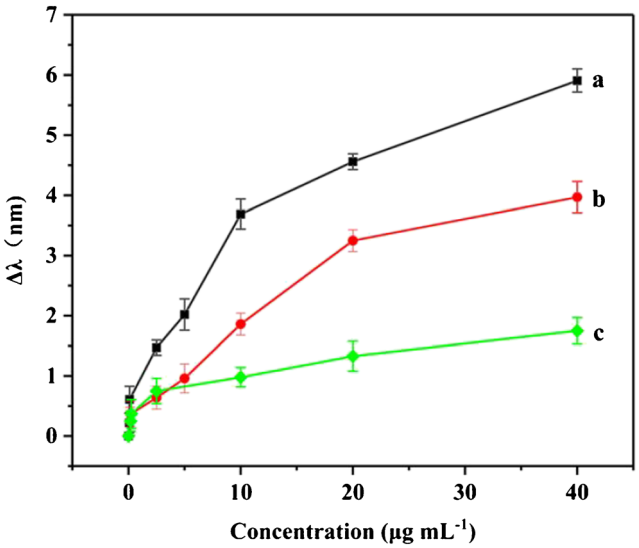

Fig. 8 Relationship between the shift of the resonant wavelengths (Δλ) and concentration of human IgG with different biosensors based on **a** PDA/Ti_3C_2-MXene/PDA-gold film, **b** PDA-gold film, and **c** bare gold film. Error bar = ±SD and n = 3

To ensure the stability of the assembled layer, the sensing platform was rinsed for 10 washing cycles. The negligible shift of wavelength is shown in Fig. S2, which demonstrated that the sensing platform was sufficiently stable. After the installation of the fabricated sensing film, different concentrations of Ab_1 were separately injected into the flow cell. As an increasing quantity of Ab_1 was fixed on the sensing substrate, a redshift of the wavelength (Δλ) increased gradually and reached its maximum after 40 min, indicating that immobilization was accomplished in 40 min. The Δλ increased with the increased concentration up to 90 μg mL^{-1} Ab_1. When 110 μg mL^{-1} Ab_1 was injected into the biosensor, there was little change in Δλ compared with immobilization of 90 μg mL^{-1} Ab_1. Therefore, the final optimization results shown in Fig. 4 indicate that the optimal conditions were 90 μg mL^{-1} Ab_1 incubated for 40 min, and the maximum

Table 1 Comparison of this biosensor and reported biosensors

Biosensors	LOD	References
Graphene oxide/silver-coated fiber biosensor	0.04 μg mL^{-1}	[35]
Hierarchical mesoporous silica film biosensor	10 nM (1.5 μg mL^{-1})	[36]
Multilayer AuNPs/Au film fiber biosensor	10 ng mL^{-1}	[37]
GO-SPA-modified fiber biosensor	0.5 μg mL^{-1}	[38]
Au-nanoshell-modified LRSPR biosensor	0.2 μg mL^{-1}	[39]
PDA/Ti_3C_2-MXene/PDA film biosensor	0.075 μg mL^{-1}	This work

Δλ was 8 nm. As noted above, the sensing substrate with a sandwich structure exhibited strong stability and superior antibody binding ability.

Optimization of reaction conditions

Several assay conditions were tested and optimized before formal detection began. Human IgG was injected from low to high concentrations, and the resonant peak changed very little after the concentration reached 40 μg mL^{-1} (Fig. 5a). The Δλ reached a maximum 30 min after injection of human IgG (Fig. 5b). Therefore, the upper limit of human IgG was 40 μg mL^{-1} and the optimal fixed time was 30 min.

After the binding of Ab_1 to human IgG, AuNPs/SPA/Ab_2 composites were added to the biosensing system as signal amplifiers. LSPR of suitable AuNPs can be coupled with the plasma oscillator wave on the LRSPR biosensor surface to obtain the maximum electromagnetic field enhancement. The most common method for the synthesis of composite AuNPs is a chemical reduction based on citrate for $HAuCl_4$, which was proposed by Turkevich [31] and improved by Frens [32]. To immobilize Ab_2 on AuNPs with optimal orientation, SPA was also performed owing to its selective binding ability with fragment crystallizable regions of antibodies [33]. The absorption peak of the AuNPs was located at 530 nm in the UV-Vis absorption spectrum (Fig. 6a) and that of AuNPs/SPA was located at 534 nm, demonstrating the successful synthesis of the above substances.

Next, we optimized the volume ratio of AuNPs/SPA to Ab_2, and the results are displayed in Fig. 6b. Fifty microliters of Ab_2 (1 mg mL^{-1}) was added to different volume of AuNPs/SPA, and the total volume was adjusted to 1 mL with PBS. The mixed solution was kept at 4 °C overnight and then centrifuged. The UV-Vis absorption peak intensity was correlated with the concentration of residual Ab_2 in supernatant. The quantity of unbound Ab_2 decreased with the increase in the volume of AuNPs/SPA, and there was almost no difference in intensity between 250 μL and 300 μL volumes of AuNPs/SPA. Therefore, the optimal volume ratio was 250 μL AuNPs/SPA with 50 μL Ab_2, and we adopted this optimized value in the following experiments.

Table 2 Relative response signal of LRSPR after storage for 15 and 30 days

Storage time (days)	Relative response (%)
0	100
15	92
30	80

The immunoassay of the biosensor

The last optimization performed was the ratio of AuNPs/SPA/Ab_2 to human IgG. A total of 40 μg mL^{-1} human IgG was injected after the immobilization of Ab_1. Next, 500 μL AuNPs/SPA/Ab_2 in different concentrations was injected and the Δλ values were recorded (Fig. 7). The Δλ reached a maximum when the concentration of Ab_2 was 125 μg mL^{-1}.

After all the optimization steps above were completed, different concentrations of human IgG were detected by the proposed biosensor, and the Δλ values were recorded. As shown in Fig. 8, the Δλ increased with the increased concentration of human IgG. The biosensor demonstrated a good response to human IgG from 0.075 μg mL^{-1} to 40 μg mL^{-1}, and the maximum Δλ was 6 nm. Because of the sensitivity constriction of the LRSPR instrument, the minimum Δλ that could elicit a response was 0.2 nm. The limit of quantitation (LOQ) was 0.075 μg mL^{-1} and the limit of detection (LOD) was 0.0225 μg mL^{-1}.

For comparison experiments, PDA-gold film and bare gold film were also employed as LRSPR biosensor substrates for immunoassay under the same conditions. The PDA-gold film LRSPR biosensor exhibited a good response to human IgG concentration from 0.15 μg mL^{-1} to 40 μg mL^{-1}, and the maximum

Table 3 Recovery of human IgG in bovine serum samples by the PDA/Ti_3C_2-MXene/PDA-modified LRSPR biosensor (n = 3)

Content of human IgG (μg mL^{-1})	Spiked (μg mL^{-1})	Δλ (nm)	$Δλ_{Serum}$ (nm)	Recovery (%)	RSD (%)
None	10	3.7	3.8	103	9.4
None	20	4.6	4.5	98	6.8
None	40	5.9	6.2	106	2.2

Δλ was 4 nm. The bare gold film LRSPR biosensor exhibited a good response to human IgG concentration from 0.2 μg mL^{-1} to 40 μg mL^{-1}, and the maximum Δλ was 2 nm. Therefore, the LOQ of the LRSPR biosensor based on PDA/Ti_3C_2-MXene/PDA was significantly lower than that of the PDA-gold- and bare gold-modified LRSPR biosensor. In a previous work by our team [34], the LOQ of the SPR biosensor was 1.25 μg mL^{-1}. Thus the LOQ of this novel LRSPR biosensor was about 20 times lower than the previous experimental results. In addition, we conducted an immunoassay based on the PDA/Ti_3C_2-MXene/PDA LRSPR biosensor without AuNPs for comparison. The results, as shown in Fig. 9, revealed that the amplification of Δλ was almost double when AuNPs were introduced, indicating that the coupling between LSPR and LRSPR effectively enhanced the detection sensitivity.

Table 1 lists other reported methods for the detection of human IgG, with LOQ distributed in a large range from 10 ng mL^{-1} to 1.5 μg mL^{-1}. The LOQ of this novel LRSPR biosensor was not the lowest among the reported biosensors due to the low resolution and sensitivity of the miniature spectrometer employed in the lab-built LRSPR biosensor, but a low level was still achieved. Therefore, the method adopted in this work did enhance the properties of the LRSPR biosensors.

To ensure the specificity of immunoassay, human IgG was replaced by mouse IgG and bovine IgG to conduct the experiments. The position of the resonance peak was almost unchanged (Fig. S3), indicating the good specificity of the LRSPR biosensor in immunoassay.

Stability of the sensing platform

We examined the stability of the sensing chips after 15 days and 30 days from when they were prepared. Table 2 shows the corresponding response signal for detection of 40 μg mL^{-1} human IgG. After storage for 15 and 30 days, the signal decreased 8% and 20%, respectively, representing the loss of activity. These data indicate that the sensing chips had good stability, which was partly attributable to the PDA/Ti_3C_2-MXene/PDA sandwich structure. PDA effectively prevented the oxidation of the functional group on Ti_3C_2-MXene, to maintain the stability of the LRSPR sensing platform.

Recovery analysis of spiked samples

We analyzed bovine serum samples containing different concentrations of human IgG (10, 20, and 40 μg mL^{-1}) for recovery experiments. The recovery was the ratio of $\Delta\lambda_{serum}$ from spiked serum and Δλ from PBS with the same concentration of human IgG ($\Delta\lambda_{serum}/\Delta\lambda$). Table 3 shows that the ranges of recoveries and RSDs were 98–106% and 2.2–9.4%, respectively, which indicates that this novel LRSPR biosensor performed well in immunoassay of human IgG in serum samples.

Conclusions

In this report, we proposed an LRSPR biosensor based on a PDA/Ti_3C_2-MXene/PDA-fabricated sensing platform and introduced sandwich amplification with AuNPs. The sensing platform was composed of three assembled layers, and Ti_3C_2-MXene film increased the surface area and provided additional binding sites. The sandwich structure effectively prevented the oxidation of Ti_3C_2-MXene and provided a convenient means of connection between Ti_3C_2-MXene and other materials. The detection range for human IgG was 0.075 μg mL^{-1} to 40 μg mL^{-1} and the LOD was 0.0225 μg mL^{-1}. This novel immunobiosensor expands the application of LRSPR and Ti_3C_2-MXene. Furthermore, this system could also be used to detect other biological samples such as tumor markers and bacteria.

We believe that the above-described layer modification of the sensing film can be made into a prefabricated kit, thus providing an Epi-Ready unit in order to shorten the detection process and greatly improve detection efficiency. In addition, the sensitivity and LOD of this LRSPR biosensor could be further enhanced via additional modification, for potential use in a broader range of applications.

Supplementary Information The online version contains supplementary material available at https://doi.org/10.1007/s00216-021-03858-8.

Acknowledgements This work was supported by the Science and Technology Developing Foundation of Jilin Province of China [grant number 20200404173YY].

Authorship contribution statement Xueqi Zhao: Conceptualization, methodology, validation, formal analysis, writing—original draft, writing—review & editing, visualization. Yue Zhang: Visualization, methodology. Xinghua Wang: Formal analysis. Pinyi Ma: Resources. Daqian Song: Resources. Ying Sun: Resources, conceptualization, writing—review & editing, funding acquisition, supervision.

Declarations

Conflict of interest The authors declare that they have no known competing financial interests or personal relationships that could have appeared to influence the work reported in this paper.

References

1. Shi H, Liu Z, Wang X, Guo J, Liu L, Luo L, et al. A symmetrical optical waveguide based surface plasmon resonance biosensing system. Sens Actuators B: Chem. 2013;185:91–6.
2. Sarid D. Long-range surface-plasma waves on very thin metal films. Phys Rev Lett. 1981;47(26):1927–30.
3. Mejard R, Dostalek J, Huang CJ, Griesser H, Thierry B. Tuneable and robust long range surface plasmon resonance for biosensing applications. Opt Mater. 2013;35(12):2507–13.
4. Wu L, Ling Z, Jiang L, Guo J, Dai X, Xiang Y, et al. Long-range surface Plasmon with Graphene for enhancing the sensitivity and detection accuracy of biosensor. IEEE Photonics J. 2016;8(2):1–9.

5. Wang L, Liu X-J, Hao J, Chu L-Q. Long-range surface plasmon resonance sensors fabricated with plasma polymerized fluorocarbon thin films. Sens Actuators B-Chem. 2015;215:368–72.
6. Vala M, Baldini F, Dostálek J, Homola J, Lieberman RA, Homola J, et al. Diffraction grating-coupled surface plasmon resonance sensor based on spectroscopy of long-range and short-range surface plasmons. Optical Sens Technol Appl. 2007; Prague, CZECH REPUBLIC2007.
7. Paliwal A, Sharma A, Tomar M, Gupta V. Long range surface plasmon resonance (LRSPR) based highly sensitive refractive index sensor using Kretschmann prism coupling arrangement. In: Sharma NN, Gaol FL, Akhtar J, editors. 2nd international conference on emerging technologies: Micro to Nano 2015. AIP conference proceedings. 1724. Melville: Amer Inst Physics; 2016.
8. Isaacs S, Abdulhalim I. Long range surface plasmon resonance with ultra-high penetration depth for self-referenced sensing and ultra-low detection limit using diverging beam approach. Appl Phys Lett. 2015;106(19):193701.
9. Tangkawsakul W, Srikhirin T, Shinbo K, Kato K, Kaneko F, Baba A. Application of long-range surface Plasmon resonance for ABO blood typing. Int J Anal Chem. 2016;2016:1–8.
10. Chabot V, Miron Y, Grandbois M, Charette PG. Long range surface plasmon resonance for increased sensitivity in living cell biosensing through greater probing depth. Sens Actuators B: Chem. 2012;174:94–101.
11. Wark AW, Lee HJ, Corn RM. Long-range surface plasmon resonance imaging for bioaffinity sensors. Anal Chem. 2005;77(13):3904–7.
12. Yang C-T, Wu L, Bai P, Thierry B. Investigation of plasmonic signal enhancement based on long range surface plasmon resonance with gold nanoparticle tags (vol 4, pg 9897, 2016). J Mater Chem C. 2016;4(44):10562.
13. Zhang N, Liu B, Cui X, Li Y, Tang J, Wang H, et al. Recent advances in aptasensors for mycotoxin detection: on the surface and in the colloid. Talanta. 2021;223:121729.
14. Wong WR, Sekaran Shamala D, Mahamd Adikan FR, Berini P. Detection of dengue NS1 antigen using long-range surface plasmon waveguides. Biosens Bioelectron. 2016;78:132–9.
15. Wong WR, Krupin O, Sekaran SD, Adikan FRM, Berini P. Serological diagnosis of dengue infection in blood plasma using long-range surface Plasmon waveguides. Anal Chem. 2014;86(3):1735–43.
16. Loyez M, Lobry M, Hassan EM, DeRosa MC, Caucheteur C, Wattiez R. HER2 breast cancer biomarker detection using a sandwich optical fiber assay. Talanta. 2021;221:121452.
17. Krupin O, Wong WR, Mahamd Adikan FR, Berini P. Detection of small molecules using long-range surface Plasmon Polariton waveguides. IEEE J Select Topics Quantum Electronics. 2017;23(2):103–12.
18. Wu Q, Li N, Wang Y, Liu Y, Xu Y, Wei S, et al. A 2D transition metal carbide MXene-based SPR biosensor for ultrasensitive carcinoembryonic antigen detection. Biosens Bioelectron. 2019;144:111697.
19. Wu L, Guo J, Wang Q, Lu S, Dai X, Xiang Y, et al. Sensitivity enhancement by using few-layer black phosphorus-graphene/TMDCs heterostructure in surface plasmon resonance biochemical sensor. Sens Actuators B: Chemical. 2017;249:542–8.
20. Barsoum MW. The M(N+1)AX(N) phases: a new class of solids; thermodynamically stable nanolaminates. Prog Solid State Chem. 2000;28(1–4):201–81.
21. Wu Q, Li N, Wang Y, Xu Y, Wu J, Jia G, et al. Ultrasensitive and selective determination of Carcinoembryonic antigen using multifunctional ultrathin amino-functionalized Ti3C2-MXene Nanosheets. Anal Chem. 2020;92(4):3354–60.
22. Wang H, Li H, Huang Y, Xiong M, Wang F, Li C. A label-free electrochemical biosensor for highly sensitive detection of gliotoxin based on DNA nanostructure/MXene nanocomplexes. Biosens Bioelectron. 2019;142:111531.
23. Chen J, Tong P, Huang L, Yu Z, Tang D. Ti3C2 MXene nanosheet-based capacitance immunoassay with tyramine-enzyme repeats to detect prostate-specific antigen on interdigitated micro-comb electrode. Electrochim Acta. 2019;319:375–81.
24. Liu H, Zhang X, Zhu Y, Cao B, Zhu Q, Zhang P, et al. Electrostatic self-assembly of 0D–2D SnO2 quantum dots/Ti3C2Tx MXene hybrids as anode for Lithium-ion batteries. Nano-Micro Letters. 2019;11(1):65.
25. Li W, Song Z, Zhong J, Qian J, Tan Z, Wu X, et al. Multilayer-structured transparent MXene/PVDF film with excellent dielectric and energy storage performance. J Mater Chem C. 2019;7(33):10371–8.
26. Chen F, Wu Q, Song D, Wang X, Ma P, Sun Y. Fe3O4@PDA immune probe-based signal amplification in surface plasmon resonance (SPR) biosensing of human cardiac troponin I. Colloids Surf B: Biointerfaces. 2019;177:105–11.
27. Park C, Kang J, Baek I, You J, Jang K, Na S. Highly sensitive and selective detection of single-nucleotide polymorphisms using gold nanoparticle MutS enzymes and a micro cantilever resonator. Talanta. 2019;205:10.
28. Akgonullu S, Yavuz H, Denizli A. SPR nanosensor based on molecularly imprinted polymer film with gold nanoparticles for sensitive detection of aflatoxin B1. Talanta. 2020;219:121219.
29. Wu Q, Song D, Zhang D, Zhang H, Ding Y, Yu Y, et al. A highly sensitive SPR biosensor based on a graphene oxide sheet modified with gold bipyramids, and its application to an immunoassay for rabbit IgG. Microchim Acta. 2015;182(9–10):1739–46.
30. Jing J-Y, Wang Q, Zhao W-M, Wang B-T. Long-range surface plasmon resonance and its sensing applications: a review. Opt Lasers Eng. 2019;112:103–18.
31. Turkevich J, Hillier J, Stevenson PC. The nucleation and growth processes in the synthesis of colloidal gold. Discuss Faraday Soc. 1951;11:55–75.
32. Frens G. Controlled nucleation for the regulation of the particle size in Monodisperse gold suspensions. Nature. 1973;241(105):22.
33. Tang DP, Yuan R, Chai YQ. Novel immunoassay for carcinoembryonic antigen based on protein A-conjugated immunosensor chip by surface plasmon resonance and cyclic voltammetry. Bioprocess Biosyst Eng. 2006;28(5):315–21.
34. Zhang H, Sun Y, Gao S, Zhang J, Zhang H, Song D. A novel Graphene oxide-based surface Plasmon resonance biosensor for immunoassay. Small. 2013;9(15):2537–40.
35. Wang Q, Wang B-T. Surface plasmon resonance biosensor based on graphene oxide/silver coated polymer cladding silica fiber. Sens Actuators B-Chemical. 2018;275:332–8.
36. Li J, Lu D-f, Zhang Z, Liu Q, Qi Z-m. Hierarchical mesoporous silica film modified near infrared SPR sensor with high sensitivities to small and large molecules. Sens Actuators B-Chem. 2014;203:690–6.
37. Xia F, Song H, Zhao Y, Zhao WM, Wang Q, Wang XZ, et al. Ultra-high sensitivity SPR fiber sensor based on multilayer nanoparticle and au film coupling enhancement. Measurement. 2020;164:9.
38. Wang Q, Jing JY, Wang BT. Highly sensitive SPR biosensor based on Graphene oxide and staphylococcal protein a co-modified TFBG for human IgG detection. IEEE Trans Instrum Meas. 2019;68(9):3350–7.
39. Cheng Z, Wang Q, Zhu A-s, Qiu F-m, Niu L-Y, Jing J-Y. Au-nanoshells modified surface field enhanced LRSPR biosensor with low LOD for highly sensitive hIgG sensing. Opt Laser Technol. 2021;134:106656.